energies

MDPI

Article

The Impact of Grid-Forming vs. Grid-Following Converters on Frequency Regulation: Comparing Centralised or Distributed Photovoltaic Generation

Giuseppe Marco Tina [1], Giovanni Maione [1,*] and Domenico Stefanelli [2]

[1] Dipartimento di Ingegneria Elettrica, Elettronica e Informatica, Università degli Studi di Catania, 95125 Catania, Italy; giuseppe.tina@unict.it
[2] Enel Energy and Commodity Management Italia, 00198 Roma, Italy; domenico.stefanelli@enel.com
* Correspondence: giovanni.maione@phd.unict.it

Abstract: Energy transition strategies point to energy systems that rely mostly on renewable sources, with photovoltaics being the most commonly used and emphasised. The transition from the past to the future of electrical system is characterised by the contrast between centralised and distributed generation, as well as the differences between synchronous machines and static converters and thus by their way to deliver services required for proper system operation, frequency regulation and transient stability. This paper compares the two converter control strategies, grid following and grid forming, for providing frequency regulation service while considering bulk photovoltaic generation at the HV level and MV-connected distributed by PV generation. The analyses reveal the equivalence between large plants and distributed resources for frequency regulation purposes, highlighting the relevance of grid-forming converter and their ability to supply inertia to the system. These results are obtained for the IEEE 14-bus system implemented in Dig Silent PowerFactory.

Keywords: frequency regulation; distributed generation; grid-forming inverters

Citation: Tina, G.M.; Maione, G.; Stefanelli, D. The Impact of Grid-Forming vs. Grid-Following Converters on Frequency Regulation: Comparing Centralised or Distributed Photovoltaic Generation. *Energies* **2024**, *17*, 5827. https://doi.org/10.3390/en17235827

Academic Editor: Miguel Castilla

Received: 17 October 2024
Revised: 13 November 2024
Accepted: 19 November 2024
Published: 21 November 2024

1. Introduction

During the past year, the ongoing energy transition has resulted in a 473 GW (+13.9%) growth in worldwide renewable energy sources (RESs) capacity, reaching 3870 GW by the end of 2023. With a capacity of 1419 GW, solar energy accounts for the largest share of renewable energy sources with a considerable growth of 346 GW (+32.2%) [1]. The rapid expansion of photovoltaic (PV) is likely facilitated by its modularity, which enables big, medium and small PV generating plants to be connected to both transmission and distribution grids. As additional RESs are integrated into the electrical power system (EPS), the number of inverter-based resources (IBRs) increases while the number of synchronous generators (SGs) decreases.

Technical differences among IBRs and traditional SGs [2,3] introduce new challenges for transmission system operators (TSOs), which have to develop new strategies and investments for the management of transmission networks. At the same time, transitions are also affecting distribution networks and its interaction with the transmission systems, due to the spread of distributed generation (DG) and distributed energy resources (DERs). In this context, it is important to take into account the stability of an EPS [4–6] that is ensured by the so-called ancillary services, which are necessary for the proper functioning of the system, ensuring continuity, quality and security of the electricity supply service [7,8]. In a traditional EPS, only SGs provide ancillary services managed by TSOs, while distribution system operators (DSOs) have a passive role, focused on guaranteeing the supply of electricity to consumers.

With the transition process, RESs in the form of large plants, connected to the transmission system (HV level) or DG, DERs connected to distribution grids (MV or LV level)

will, on one hand, lead to the gradual decommissioning of conventional SGs with the consequent reduction in capacity for the provision of ancillary services; on the other hand, they represent potential new sources of flexibility for both TSOs and DSOs to manage the EPS [9]. In terms of frequency stability, it is widely understood that the non-programmability of primary energy sources, which distinguishes RESs, causes criticalities in the balance of consumption and production, resulting in frequency changes. Another drawback is that RES generators constantly run at their maximum power point (MPP), extracting the maximum available energy, resulting in no energy reserves to provide frequency regulation services. In this sense, an important contribution can be made by the battery energy storage systems (BESSs) in terms of energy time-shifting and provision of ancillary services [10,11]. Another issue for frequency stability (and system stability in general) is that, as the name implies, IBRs interface with the network via static converters which, unlike SGs, have no physical inertia that is beneficial to the system. A decrease in system inertia causes more abrupt transients, which result in higher RoCoF and lower frequency nadir (larger Zenit) values [12,13].

Despite these differences, the possibility for various control methods for static converters provide a high degree of flexibility to IBRs, which is an essential characteristic for future EPS. Today's inverters are divided into two broad families: grid following (GFL) and grid forming (GFM). The former account for the vast majority of inverters currently used for RES applications, whereas the latter are undergoing rapid development and is an area of growing interest among industry professionals and academics. Table 1 shows a brief comparison between the two inverter control methods, highlighting their main advantages and disadvantages. An important distinction between these two types of inverters is that the GFL approach assumes that the grid to which they are connected to can supply stable voltage and frequency, whereas GFM inverters can supply and sustain stable quantities even on weak grids. Therefore, the decommissioning of SGs must be complemented with the integration of GFM-type IBRs capable of maintaining adequate levels of system safety [14,15]. A noteworthy property of GFM inverters regards the possibility to provide power abruptly, simulating the inertia of SGs. For this reason, one of the possible controls for GFM inverters is known as virtual synchronous machine (VSM) control, and the inertia they give is known as synthetic inertia [15–17]. Numerical simulations are an important tool to support research, especially for large EPS analyses, where it is important to understand how different models interact with each other at a system level, involving studies of the whole network to highlight their potential and correct undesirable behaviours if present. This is why the use of specialised software such as DigSilent PowerFactory (2023 SP5) is used.

Table 1. Comparison of GFL and GFM inverter: Pros and Cons.

	Grid Following (GFL)	**Grid Forming (GFM)**
Pros	Simple control structure Bigger size	Creates its own voltages Able to operate in an islanded mode Able to work in weak grids Black start and inertia provision
Cons	Follow grid voltages Unable to operate in an islanded mode Instability in weak grids No black start and inertia provision	Instability in stiff grids Easily susceptible to overload Smaller size

The literature contains studies on the usage of RES to provide frequency regulation services; for example, in [18], the authors investigated the frequency impact of HV grid-connected wind power plants capable of generating synthetic inertia. In [19,20], PV systems were used to provide frequency services in small grids without the usage of energy storage. In contrast, ref. [21] considers a BESS attached to the PV generator for the aim of delivering frequency services to increase system stability. The work proposed in [22] focusses on

the use of a BESS to provide frequency regulation services, comparing centralised and distributed systems. Although in recent years, storage has been emphasised as the main solution to the RES integration problem; the power management of PV system, or RES in general, is a useful method that can contribute power and alleviate issues coming from the variability typical of a RES-based power system, even with limited additional cost.

For the authors, the current research is a continuation of what was conducted in [23], where dynamic analyses was performed on a system with a significant presence of IBRs to study the effectiveness of droop control and virtual synchronous machine algorithms for GFM inverters.

The authors are not aware of any work on frequency stability considering different inverter technologies, such as GFL and GFM, comparing centralised and distributed PV generation. Therefore, the innovative contribution of this work is to compare the provision of frequency regulation services by large PV plants, connected to the HV grid, and distributed plants, on the MV side, considering both GFL- and GFM-type inverters. These analyses were carried out with the DigSilent PowerFactory software on the IEEE 14-bus system.

In accordance with the expected significant development of renewable energies, especially photovoltaics, studies such as this one are required to understand how new technologies can provide services to the grid and how these services can evolve. Furthermore, this study is in line with the current push for collaboration between TSOs and DSOs to build efficient and robust grids. TSOs rely on DSOs to coordinate and manage resources in their networks, both as individual units and as aggregates, in order to make them available for the provision of valuable system services, allowing TSOs to utilise these additional resources as needed.

The remainder of the paper is organised as follows. Section 2 describes the utilised test system and how the analyses and simulation are conducted on it. Next, Section 3 provides the simulation results comparing the various studied cases. Finally, Section 4 presents the main conclusion of this paper.

2. System Description and Methodology

In this section some details about the test system used in this work and the methodology used for the simulations are given.

2.1. System Description

Thanks to the modest number of busses, the IEEE 14-bus system is used for different steady-state and dynamic studies. In the literature, it has already been used to analyse different system features: in [24,25] the weakest busses were determined; in [26] transient stability analyses were performed by considering the rotor angle after a short circuit event; in [27] three phase short circuits, the generator and load busses were analysed to show the impact of different fault location on the voltage profiles; a comparison between STATCOM and VSM-STATCOM, for voltage and frequency stability, was performed in [28]; finally in [18] analyses on frequency stability were developed using GFL and GFM converters capable of providing synthetic inertia and a new control of GFL is proposed for this goal.

The IEEE 14-bus system represents the Midwest United States grid using a simple model that includes transmission and distribution networks, considering four voltage levels, as shown in Figure 1. The number of synchronous machines in the system is five, two of these work as generators, Gen1 and Gen2, while the other three are operated as synchronous compensator. The size, inertia and droop coefficient of the machines present in the system are reported in Table 2, while the load flow results summary for the IEEE 14-bus system is reported in Table 3. A more complete description of the system is presented in [26,29].

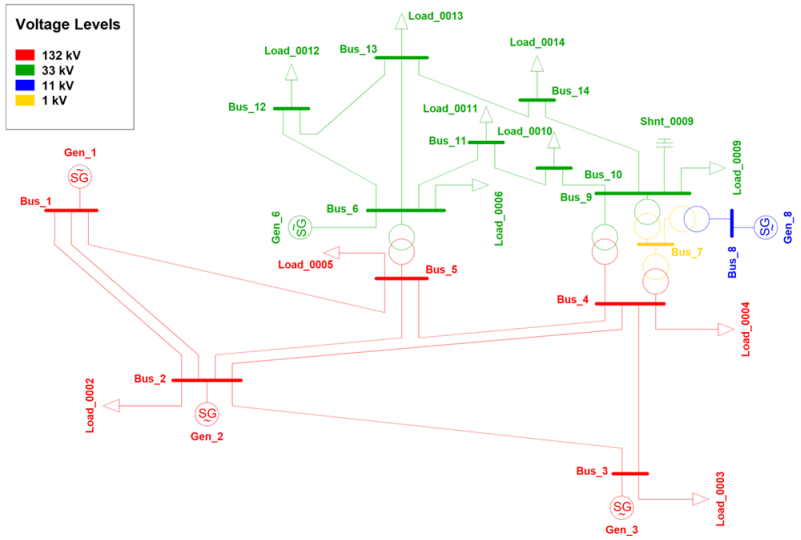

Figure 1. IEEE 14-Bus System.

Table 2. Synchronous Generators Size, Inertia and droop.

	Gen_1	Gen_2	Gen_3	Gen_6	Gen_8
Size [MVA]	615	60	60	25	25
H [s]	5.148	6.54	6.54	5.06	5.06
Droop [%]	5	5	-	-	-

Table 3. IEEE 14-bus load flow results summary.

Gen MW	Gen MVAr	Load MW	Load MVAr	Loss MW	Loss MVAr
272.74	82.47	259.00	73.50	13.74	28.59

2.2. Methodology

This research work has the dual objective of comparing frequency transients in cases where the frequency regulation service is provided as follows:

- A conventional PV generation system based on GFL inverters or a system using GFM inverters;
- A centralised generation (CG) system consisting of a large PV plant connected at HV level or distributed PV generators (DG) connected at MV level.

To this end, three scenarios were developed using the IEEE 14-bus system present in the DigSilent PowerFactory library [29].

The Base scenario involves the use of the IEEE 14-bus network as it is, consisting only of synchronous generators, with no presence of RESs. To account for the presence of RES generation, the PV-GFL and PV-GFM scenarios are created by replacing the Gen2 with a HV-connected bulk PV plant or through MV-connected distributed PV plants, using GFL and GFM technology, see Table 4 for a brief summary. Concerning GFL type, the large scale PV plant of 60 MW is connected at HV level to the same bus of the Gen2, i.e., bus2; this is conducted using the model WECC large-scale PV plant REPC_A [30], see Appendix A; for the distributed generation case, there are 6 PV systems of 10 MW connected at MV level (33 kV) to busses 9, 10, 11, 12, 13 and 14; these plants are implemented using the WECC DER system DER_A [31], see Appendix B. Regarding the case of PV system with GFM inverter, they are implemented using the DigSilent template model virtual synchronous machine [32], see Appendix C.

Table 4. Generation type and PV models used in the scenarios.

Scenario	Generation Type		PV Model	
	Gen_1	Gen_2	Centralised	Distributed
Base	SG	SG	-	-
PV-GFL	SG	PV-GFL	WECC Large-scale PV	WECC DER System
PV-GFM	SG	PV-GFM	DigSilent GFM VSM	DigSilent GFM VSM

In this work, the PV systems are working at lower than their maximum power point (MPP); this allows the PV generator to have a power reserve that can be exploited in case of underfrequency transients. To participate in frequency regulation, an upward droop of 4.6% and downward droop of 2.6% has been assigned to the PV generators and a frequency deadband of 200 mHz is considered, as indicated in [33,34]. The synthetic inertia of a GFM inverter is set to 3 s.

To analyse how frequency transients evolve, three different contingencies are applied to these scenarios: under and over-frequency due to power imbalance and synchronous power generation outage.

The power imbalances are implemented as follows:

- Under frequency case: load demand variations (DL) of +10%, +15% and +20% of the total load active power (constant power factor), once as a variation in a single HV load, load 3, and the other as a variation in the loads connected to the 33 kV MV distribution network;
- Over-frequency case: load demand variations (DL) of −10%, −15% and −20% of the total load active power (constant power factor), once as a variation in a single HV load, load 3, and the other as a variation in the loads connected to the 33 kV MV distribution network.

Concerning the event of generator outage:

- Generation outage case: Gen1 is considered as a power plant composed of a group of machines at which the loss of 25%, 33% and 50% of the plant is tested.

For each scenario considered and for each contingency case analysed, frequency and active power results have been obtained from numerical dynamic simulations using the DigSilent's "Simulation RMS" tool:

- Step size of 0.05 s
- Contingency occurs at t = 1 s
- Simulation time is 30 s.

The system inertia and the expected RoCoF values ($RoCoF_{exp}$) have been calculated using Equation (1) presented in [35,36], while the actual values $RoCoF_{act}$ is taken from the simulation results of "Derivative of El. Frequency in p.u./s".

$$H = \frac{\sum_i^N H_i \cdot S_{G,i}}{\sum_i^N S_{G,i}}; \quad RoCoF_{t=0^+} = \frac{\Delta P_{Umbalance}}{S_{Gtot}} \frac{f_0}{2H} \tag{1}$$

Other values such as frequency nadir, steady-state frequency, rise time and settling time are obtained as outputs of the Matlab's function "Stepinfo", using the frequency data collected as the input in the DigSilent simulations.

The differences in frequency nadir values, ef_{Nadir}, and steady-state frequencies, $ef_{SS}0$, obtained for the case of HV or MV imbalance have been calculated in percentage using (2), taking the values of the HV case as reference. The deviation of nadir and steady-state frequencies between the HV centralised and the MV distributed PV case have been calculated using (3), taking the PVHV case as reference.

$$ef_{Nadir} = 100\frac{f_{Nadir}^{MV} - f_{Nadir}^{HV}}{f_{Nadir}^{HV}}; \; ef_{SS} = 100\frac{f_{SS}^{MV} - f_{SS}^{HV}}{f_{SS}^{HV}} \tag{2}$$

$$ef_{Nadir} = 100\frac{f_{Nadir}^{PVMV} - f_{Nadir}^{PVHV}}{f_{Nadir}^{PVHV}};\ ef_{SS} = 100\frac{f_{SS}^{PVMV} - f_{SS}^{PVHV}}{f_{SS}^{PVHV}} \quad (3)$$

The frequency results of each scenario are then shown together to compare the obtained values. A plot of the generators active power output is shown to determine the differences in their power response.

3. Simulations and Results

3.1. Unbalance Underfrequency Case

The first analysed transient concerns the underfrequency caused by the load increase described in the Methodology paragraph. The frequency results obtained for the Base scenario are summarised in Table 5, where the reported data show a comparison between the load variation occurring at HV and MV levels. The last two columns show the difference in percentage between the frequency nadir and steady-state frequency obtained for the case of HV or MV unbalance.

Table 5. Base Scenario; Frequency results for the unbalance underfrequency case.

	Inertia [s]	$RoCoF_{exp}$ [Hz/s]	$RoCoF_{act}$ [Hz/s]	f_{Nadir} [Hz]	RiseTime [s]	SettlingTime [s]	f_{SS} [Hz]	ef_{Nadir} [%]	ef_{SS} [%]
DL10% HV	5.355	0.154	0.189	49.811	0.750	7.650	49.862		
DL10% MV	5.355	0.154	0.188	49.814	0.745	7.657	49.865	0.006	0.005
DL15% HV	5.355	0.231	0.285	49.715	0.750	7.643	49.792		
DL15% MV	5.355	0.231	0.284	49.719	0.741	7.648	49.796	0.009	0.007
DL20% HV	5.355	0.308	0.382	49.617	0.748	7.635	49.721		
DL20% MV	5.355	0.308	0.382	49.623	0.737	7.636	49.726	0.012	0.011

As can be expected with equal system inertia, the bigger the unbalance the more serious the underfrequency event; this results in a lower frequency nadir (f_{Nadir}), lower steady-state frequency (f_{SS}) and higher RoCoF. The very small values of ef_{Nadir} and ef_{SS} confirm that frequency problems are global and affect the whole system, allowing us to consider the HV or MV load change case indifferently, such as the HV case that has been chosen here. Furthermore, the following analyses only consider the most severe unbalance, i.e., a 20% load change.

Considering the PV-GFL scenario, the cases of a large HV-connected PV plant and distributed PV generation are compared. The obtained frequency results reported in Table 6 show that there are no clear differences between the case of centralised and distributed PV generation, efNadir, efSS ~0%. For this reason, here the focus is on distributed PV systems when comparing GFL and GFM technology. Therefore, in Table 7 the PV-GFM scenario results are compared to those of the Base and PV-GFL scenarios.

Table 6. PV-GFL Scenario, Frequency results for the DL20% HV unbalance underfrequency case, PVHV and PVMV comparison.

	Inertia [s]	$RoCoF_{exp}$ [Hz/s]	$RoCoF_{act}$ [Hz/s]	f_{Nadir} [Hz]	RiseTime [s]	SettlingTime [s]	f_{SS} [Hz]	ef_{Nadir} [%]	ef_{SS} [%]
PVHV	4.855	0.340	0.430	49.574	0.688	9.671	49.705		
PVMV	4.855	0.340	0.442	49.570	0.670	9.605	49.706	−0.008	0.003

Among the studied scenarios, the PV-GFL ones experiences the sudden frequency transient, showing the higher RoCoF, frequency nadir and the lower rise time, reaching the final frequency value after a longer settling time. This is due to the lower system inertia caused by the substitution of the SG Gen2 with IBR that is not capable of providing synthetic inertia, such as GFL inverters. In contrast, in the PV-GFM scenario the replacement of Gen2 has less impacts on the frequency transient thanks to the provision of synthetic inertia by

GFM-type inverters. In this case, the inertia is higher than the one in the PV-GFL scenario, which is trying to catch up to the inertia of the Base scenario.

Table 7. Frequency result for the DL20% HV unbalance underfrequency case distributed PV, Scenarios comparison.

	Inertia [s]	$RoCoF_{exp}$ [Hz/s]	$RoCoF_{act}$ [Hz/s]	f_{Nadir} [Hz]	RiseTime [s]	SettlingTime [s]	f_{SS} [Hz]
Base	5.355	0.308	0.382	49.617	0.748	7.635	49.721
PV-GFL	4.855	0.340	0.442	49.570	0.670	9.605	49.706
PV-GFM	5.085	0.324	0.422	49.601	0.741	7.530	49.705

When the results of the Base and PV-GFM scenarios are compared, the frequency nadir and RoCoF values are nearly identical, as well as rising time and settling time. The difference in steady-state frequencies among the scenarios are due to the different characteristics of the generators for primary frequency regulation. PV generators have been implemented with a different droop characteristic than SGs, considering a frequency dead band of 200 mHz. These differences in frequency between the three scenarios reflect the diverse active power curves of the generators as shown in Figure 2.

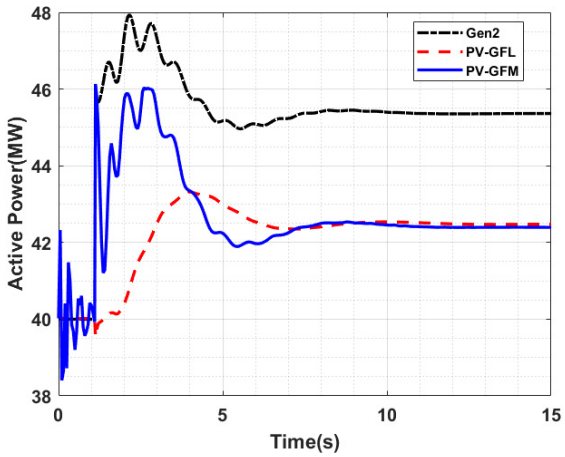

Figure 2. Generators active power, Unbalance underfrequency case, Scenarios comparison.

The active power of the SG Gen2 and the PV-GFM generator have very similar transient behaviours, providing an inertial response during the initial transient period, whereas the PV-GFL output power gives no inertial contribution and starts to deliver active power according to its droop, participating to primary frequency regulation.

The different steady state frequency values obtained in the PV-GFL and PV-GFM scenarios as compared to the Base scenario are due to the different power responses of the PV generators. Unlike the SG, they start to release power according to their droop but only for frequency outside the chosen deadband leading to a lower power output.

3.2. Unbalance Over-Frequency Case

The same analysis made in the previous section will be applied here to the case of a demand reduction that results in a generation surplus and consequently an over-frequency transient. Contrary to the case of underfrequency, in this case the contribution to frequency regulation is downward so the PV generators do not need to operate while considering a power reserve but can also work at MPP.

Table 8 shows the results of the Base scenario simulations. Again, tightening up the contingency causes higher RoCoF values and maximum frequencies, fzenit, as well as higher new steady state frequency, fSS.

Table 8. Base scenario, Frequency results for the unbalance over-frequency case.

	$RoCoF_{exp}$ [Hz/s]	$RoCoF_{act}$ [Hz/s]	f_{Zenit} [Hz]	RiseTime [s]	SettlingTime [s]	f_{SS} [Hz]	ef_{Zenit} [%]	ef_{SS} [%]
DL10% HV	0.154	0.185	50.184	0.751	7.669	50.134		
DL10% MV	0.154	0.184	50.182	0.751	7.673	50.133	−0.005	−0.003
DL15% HV	0.231	0.276	50.275	0.751	7.673	50.200		
DL15% MV	0.231	0.275	50.271	0.752	7.678	50.198	−0.007	−0.004
DL20% HV	0.308	0.367	50.364	0.751	7.677	50.265		
DL20% MV	0.308	0.365	50.360	0.752	7.682	50.263	−0.009	−0.005

Focusing on the DL20% HV case, Table 9 displays the comparison of centralised and distributed PV systems for the PV-GFL Scenario. As with the underfrequency case, the PVHV system contributes equally to frequency regulation as the PVMV system, obtaining practically the same frequency results.

Table 9. PV-GFL scenario, Frequency results for the DL20% HV unbalance overfrequency case, PVHV and PVMV comparison.

	$RoCoF_{exp}$ [Hz/s]	$RoCoF_{act}$ [Hz/s]	f_{Zenit} [Hz]	RiseTime [s]	SettlingTime [s]	f_{SS} [Hz]	e f_{Zenit} [%]	e f_{SS} [%]
PVHV	0.340	0.410	50.396	0.675	9.436	50.274		
PVMV	0.340	0.424	50.402	0.658	9.585	50.273	0.010	−0.002

Considering the distributed PV generation, the PV-GFM scenario is analysed and compared with the previous two, see Table 10. As might be expected, the inertial response of the SGs in the Base and PV-GFM scenarios aids the system in containing the frequency Zenith value, as well as the RoCoF and the rise time. Whereas the presence of GFL-type converters that cannot provide inertial contribution results in faster frequency variations showing the higher RoCoF, fzenit and the lower rise time. Although, the fSS is equal for the two PV scenarios, for the PV-GFL case the settlement of the steady-state values is obtained 2 s later.

Table 10. Frequency result for DL20% HV unbalance overfrequency case, Distributed PV, Scenarios comparison.

	$RoCoF_{exp}$ [Hz/s]	$RoCoF_{act}$ [Hz/s]	f_{Zenit} [Hz]	RiseTime [s]	SettlingTime [s]	f_{SS} [Hz]
Base	0.308	0.367	50.364	0.751	7.677	50.265
PV-GFL	0.340	0.424	50.402	0.658	9.585	50.273
PV-GFM	0.324	0.372	50.365	0.721	7.193	50.274

The output power profiles of the generators are displayed in Figure 3.

3.3. Generation Outage Case

This last case study aims to examine how the frequency of the system under examination changes in the event of a generation outage, causing the loss of part of the synchronous generation. When this occurs, the system experiences a frequency transient with depleted resources, resulting in diminished inertia and regulation capability.

Starting the analyses with the Base scenario, the system is stressed by three different rates of generation outage, see Methodology paragraph, and the resulting frequency transient values are summarised in Table 11. Looking at the inertia values, it is immediately clear that as the percentage of generation out-of-service increases, the system inertia decreases, causing more severe frequency transients, higher RoCoF and lower frequency nadir, potentially leading to system operation problems.

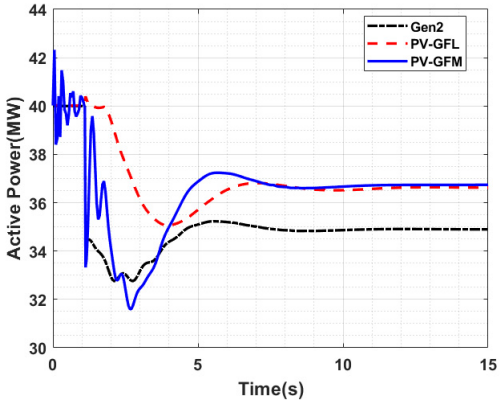

Figure 3. Generators active power, Unbalance overfrequency case, Scenarios comparison.

Table 11. Base scenario, Frequency results for the generation outage case.

	Inertia [s]	$RoCoF_{exp}$ [Hz/s]	$RoCoF_{act}$ [Hz/s]	f_{Nadir} [Hz]	RiseTime [s]	SettlingTime [s]	f_{SS} [Hz]
GenOut 25%	4.347	0.426	0.576	49.539	0.815	7.828	49.653
GenOut 33%	4.011	0.616	0.836	49.303	0.873	8.455	49.473
GenOut 50%	3.339	1.110	1.523	48.608	1.050	8.734	48.903

To study what happens if the system does not consist of synchronous generation only but also contains RES generation, and thus IBRs, the PV-GFL scenario is analysed. For this scenario, the results are shown in Table 12, for the GenOut50 case only, as comparison between the case in which Gen2 is replaced with a large HV-connected PV plant and the case of replacement by PV distributed generation.

Table 12. PV-GFL scenario, Frequency results for the GenOut 50% generation outage case, PVHV and PVMV comparison.

	Inertia [s]	$RoCoF_{exp}$ [Hz/s]	$RoCoF_{act}$ [Hz/s]	f_{Nadir} [Hz]	RiseTime [s]	SettlingTime [s]	f_{SS} [Hz]	ef_{Nadir} [%]	ef_{SS} [%]
PV HV	2.839	1.306	1.804	48.562	0.755	8.096	48.966		
PV MV	2.839	1.306	1.788	48.540	0.752	8.266	48.957	−0.045	−0.019

The differences between the PVHV and PVMV case are minimal, the PVMV seems to be the better case showing lower RoCoF and nadir, confirming the equivalence of centralised and distributed generation for this test system. Due to these results the comparison of GFL and GFM technology are made considering the case of distributed generation. In Table 13, the results of the PV-GFM scenario are reported with those of the Base and PV-GFL scenarios. Comparing these data, it is evident that thanks to the higher inertia, the Base and PV-GFM scenario have lower RoCoF and higher frequency nadir when compared to those of the PV-GFL scenario. However, in all three scenarios, the gradient of frequency variation is RoCoF > 1 Hz/s, and is a deterministic limit by ENTSOe, above which transients are considered not manageable by system protections [35,37].

In the case of generation outage, the frequency nadir of the PV-GFM scenario is even higher than the one resulting from the Base scenario. This can be explained by looking at Figure 4, where the active power responses of the generators are plotted.

The power curves show that both the SG Gen2 and PV-GFM generator have an inertia contribution that instantaneously react to the disturb event. Although, after releasing kinetic energy the Gen2 is decreasing in active power due to its capability limit (pf = 0.8), while the PV-GFM generator continues to provide additional power reaching its maximum power and producing a barely higher frequency nadir value.

Table 13. Frequency result for the GenOut 50% generation outage case, distributed PV, Scenarios comparison.

	Inertia [s]	$RoCoF_{exp}$ [Hz/s]	$RoCoF_{act}$ [Hz/s]	f_{Nadir} [Hz]	RiseTime [s]	SettlingTime [s]	f_{SS} [Hz]
Base	3.339	1.110	1.523	48.608	1.050	8.734	48.903
PV-GFL	2.839	1.306	1.788	48.540	0.752	8.266	48.957
PV-GFM	3.068	1.208	1.594	48.667	0.873	8.266	48.973

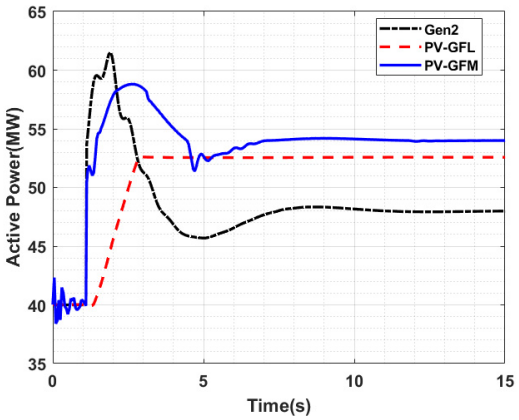

Figure 4. Generators active power, Generation outage case, Scenarios comparison.

Excluding the inertia and considering the primary frequency regulation, it can be notice that both the PV-GFL and PV-GFM generators provide a higher power than the SG Gen2, reaching a higher steady-state frequency (fSS in Table 11).

4. Conclusions

The analyses carried out in this research work showed that, for the IEEE 14-bus system, the contribution to frequency regulation of bulk resources connected in HV and distributed MV plants is practically identical, confirming the global nature of frequency problems, as opposed to voltage problems. It can therefore be concluded that MV-connected distributed generation capable of providing services is an important resource for system stability, highlighting the relevance of cooperation between the TSOs and DSOs.

Considering the comparison of PV systems based on GFL- and GFM-type inverters, it has been demonstrated that there is a need of including RESs based on GFM type IBRs into the system in order to improve the stability of EPSs that are progressively populated by static devices and the depletion of synchronous resources, thanks to their ability to emulate the behaviour of conventional SGs providing inertia and stable grid quantities. Furthermore, the responses of IBRs are dictated by their converter control. For this reason, characteristic parameters like synthetic inertia of GFM inverters can be settled as needed giving IBRs more flexibility than traditional SGs, for whom inertia is dependent on the physical size and construction of the machine. The high potential of GFM-IBRs is reflected in the continuing and growing interest of industry and academia in this type of converter control.

This work also discussed the upward regulation that PV plants could provide if they operated at a lower point than the MPP. However, if all PV plants were managed in this manner, the risk of not reaching the targets for energy demand covered by RES generation would increase, with the same amount of installed RES capacity considered as target. To meet the decarbonisation requirements while still contributing to services, more installed capacity would be required than predicted by policy scenarios. In order to achieve an environmentally friendly and above all reliable energy system, the energy transition scenarios should therefore include an incremental margin of RES capacity to compensate for the portion of energy needed as a reserve for auxiliary regulation functions.

Author Contributions: Conceptualization, G.M. and G.M.T.; methodology, G.M. and G.M.T.; software, G.M.; validation, G.M. and G.M.T.; formal analysis, G.M.; investigation, G.M.; resources, G.M. and G.M.T.; data curation, G.M.; writing—original draft preparation, G.M.; writing—review and editing, G.M., G.M.T. and D.S.; visualisation, G.M.; supervision, G.M.T. and D.S.; project administration, G.M.T. All authors have read and agreed to the published version of the manuscript.

Funding: This research was funded by PON Ricerca e Innovazione 2014–2020 Azione IV.5, grant number E69J21011500006.

Data Availability Statement: Data available on request from the authors.

Acknowledgments: This work is being carried out as part of the project "Technologies and enabling services for the green transformation of the Italian power system". The authors would like to express their gratitude to the Programma Operativo Nazionale (PON) "Ricerca e Innovazione" 2014–2020, which is sponsored by the European Social Fund, for their support and fundings, which made this research possible.

Conflicts of Interest: The authors declare no conflicts of interest.

Appendix A. REPC_A Model

Name	Value	Unit	Description
Rc	0	[p.u.]	Line drop compensation resistance
Xc	0	[p.u.]	Line drop compensation reactance
Tfltr	0.02	[s]	Voltage and reactive power filter time constant
Tp	0.02	[s]	Active power filter time constant
db	0.002	[p.u.]	Deadband in reactive power or voltage control
Kp	1	[p.u./p.u.]	Volt/VAR regulator proportional gain
Ki	5	[p.u./p.u.]	Volt/VAR regulator integral gain
Vfrz	0.7	[p.u.]	Voltage for freezing Volt/VAR regulator integrator
Tft	0	[s]	Plant controller Q output lead time constant
Tfv	0.05	[s]	Plant controller Q output lag time constant
Kc	10	[p.u.]	Reactive droop gain
FrqFlag	1		Active power control: 0 = disabled, 1 = enabled
RefFlag	1		0 = reactive power control, 1 = voltage control
VcmpFlag	0		0 = reactive droop, 1 = line drop compensation
fdbd1	−0.004	[p.u.]	Frequency deadband downside
fdbd2	0.004	[p.u.]	Frequency deadband upside
Ddn	38.46	[p.u./p.u.]	Down regulation droop gain
Dup	21.73	[p.u./p.u.]	Up regulation droop gain
Kpg	0.5	[p.u./p.u.]	Real power control proportional gain
Kig	0.35	[p.u./p.u.]	Real power control integral gain
Tlag	0.1	[s]	Plant controller P output lag time constant
emin	−0.5	[p.u.]	Minimum Volt/VAR error
Qmin	−0.436	[p.u.]	Minimum plant reactive power command
femin	−99	[p.u.]	Minimum power error in droop regulator
Pmin	0	[p.u.]	Minimum plant active power command
emax	0.5	[p.u.]	Maximum Volt/VAR error
Qmax	0.436	[p.u.]	Maximum plant reactive power command
femax	99	[p.u.]	Maximum power error in droop regulator
Pmax	0.9	[p.u.]	Maximum plant active power command

Appendix B. DER_A Model

Name	Value	Unit	Description
typeflag	0		Unit type: 0 = Generator, 1 = Storage
Trv	0.02	[s]	Transducer time constant voltage measurement
Vref0	−1	[p.u.]	Voltage reference set-point (>0; if <=0: Vref = Vt)
dbd1	−0.05	[p.u.]	Lower voltage deadband (over-voltage)
dbd2	0.05	[p.u.]	Upper voltage deadband (under-voltage)
Kqv	5	[p.u./p.u.]	Proportional voltage control gain
Tp	0.02	[s]	Transducer time constant power measurement
PfFlag	0		Control flag: 0 = Q control, 1 = power factor ctrl.
Tiq	0.02	[s]	Q control time constant
Trf	0.1	[s]	Transducer time constant frequency measurement
Freq_flag	1		Frequency control flag: 0 = disabled, 1 = enabled
Ddn	38.46	[p.u./p.u.]	Frequency control droop gain (down-side)
Dup	21.73	[p.u./p.u.]	Frequency control droop gain (up-side)
fdbd1	−0.004	[p.u.]	Lower frequency ctrl. deadband (over-freq.)
fdbd2	0.004	[p.u.]	Upper frequency ctrl. deadband (under-freq.)
Kpg	0.25	[p.u.]	Active power control proportional gain
Kig	0.5	[p.u.]	Active power control integral gain
Tpord	0.02	[s]	Power order time constant
Imax	0.9	[p.u.]	Maximum converter current
Pqflag	1		Priority for current limit: 0 = Q priority, 1 = P prio.
Tg	0.02	[s]	Current control time constant
Vtripflag	1		Voltage tripping: 0 = disabled, 1 = enabled
vl0	0.15	[p.u.]	Voltage break-point for low voltage cut-out
vl1	0.9	[p.u.]	Voltage break-point for low voltage cut-out
vh0	1.2	[p.u.]	Voltage break-point for high voltage cut-out
vh1	1.1	[p.u.]	Voltage break-point for high voltage cut-out
tvl0	0.1	[s]	Timer for low voltage break-point 0 (vl0)
tvl1	1.5	[s]	Timer for low voltage break-point 1 (vl1)
tvh0	0.1	[s]	Timer for high voltage break-point 0 (vh0)
tvh1	1.5	[s]	Timer for high voltage break-point 1 (vh1)
Vrfrac	0.7		Fraction (0. . . 1) that recovers after voltage recovery
Tv	0.02	[s]	Time constant on output of voltage cut-out
Ftripflag	1		Frequency tripping: 0 = disabled, 1 = enabled
fl	47.5	[Hz]	Frequency break-point for low freq. cut-out
fh	51.5	[Hz]	Frequency break-point for high freq. cut-out
tfl	0.3	[s]	Timer for low frequency break-point (fl) cut-out
tfh	0.3	[s]	Timer for high frequency break-point (fh) cut-out
Vpr	0.8	[p.u.]	Minimum voltage to disable frequency tripping
Iql1	−1	[p.u.]	Minimum limit of reactive current injection
femin	−99	[p.u.]	Frequency control minimum error
Pmin	0	[p.u.]	Minimum power
dPmin	−0.5	[p.u./s]	Minimum power ramp rate (down)
Iqh1	1	[p.u.]	Maximum limit of reactive current injection
femax	99	[p.u.]	Frequency control maximum error
Pmax	0.9	[p.u.]	Maximum power
dPmax	0.5	[p.u./s]	Maximum power ramp rate (up)
rrpwr	0.5	[p.u./s]	Max. power rise ramp rate following a fault

Appendix C. GFM VSM Model

Table A1. VSM.

Name	Value	Unit	Description
Ta	6	[s]	Acceleration time constant
Dp	21.73	[p.u.]	Damping coefficient
w_c	6	[rad/s]	Damping filter cut-off frequency
T_LPF_u	0.003	[s]	Voltage setpoint low-pass filter time constant
ured	0.8	[p.u.]	Voltage threshold, under-voltage Pset red.&lim.
ModeRed	1		Under-voltage Pset reduction: 0 = no; 1 = yes if output in limit
ModeLim	1		Under-voltage Pset limitation: 0 = no, 1 = linear; 2 = squared
mp_ollim	0.1		Overload limiter gain
f_setpoint	1	[p.u.]	Initial speed setting
pmin	0	[p.u.]	Minimum power
pmax	0.9	[p.u.]	Maximum power

Table A2. DC Link.

Name	Value	Unit	Description
T_cap	1000	[s]	DC capacitor time constant (capacitance)
ploss_nld	1	[%]	Inverter no-load losses (at udc = 1 p.u.)
ploss_ld	0	[%]	Inverter load losses (at pac = 1 p.u.)
ploss_sw	0	[%]	Inverter switching losses (at pac = 1 p.u.)
E_chopper_max	2	[p.u.*s]	Max. admissible chopper energy
udc_min	0.5	[p.u.]	Minimum operational DC voltage
udc_max	1.5	[p.u.]	Maximum DC voltage (chopper activation)

Table A3. FSM.

Name	Value	Unit	Description
FSM_on	0		Frequency Sensitive Mode (FSM): 0 = off, 1 = on
Mode_Db	1		Frequency deadband FSM: 0 = without, 1 = with
f_db1	−200	[mHz]	Lower frequency deadband FSM (neg. value)
f_db2	200	[mHz]	Upper frequency deadband FSM (pos. value)
delay_init_fsm	0	[s]	Initial response delay FSM (deadband)
s1	0	[%]	Droop 1 (FSM upward regulation, for f < fn)
s2	0	[%]	Droop 2 (FSM downward regulation, for f > fn)
LFSMO_on	1		Limited FSM-O (overfrequency): 0 = off, 1 = on
f1_lfsmo	50.2	[Hz]	Frequency threshold for LFSM-O (> fn)
delay_init_lfsmo	0	[s]	Initial response delay LFSM-O
s3	2.6	[%]	Droop 3 (LFSM-O downward regulation, for f > f1)
LFSMU_on	1		Limited FSM-U (underfrequency): 0 = off, 1 = on
f2_lfsmu	49.8	[Hz]	Frequency threshold for LFSM-U (<fn)
delay_init_lfsmu	0	[s]	Initial response delay LFSM-U
s4	4.6	[%]	Droop 4 (LFSM-U upward regulation, for f < f2)
T_smooth	0.02	[s]	Output smoothing time constant (PT1 filter)
dP_fsm_min	−10	[%]	Minimum additional power FSM (dP < 0)
ddP_fsm_min	−4	[%/s]	Min. rate of change in dP FSM (neg.)
dP_lfsmo_min	−100	[%]	Max. power reduction LFSM-O (dP < 0)
ddP_lfsmo_min	−100	[%/s]	Min. rate of change in dP LFSM-O
ddP_lfsmu_min	−100	[%/s]	Min. rate of change in dP LFSM-U
dP_fsm_max	10	[%]	Maximum additional power FSM (dP > 0)
ddP_fsm_max	4	[%/s]	Max. rate of change in dP FSM (pos.)
ddP_lfsmo_max	100	[%/s]	Max. rate of change in dP LFSM-O
dP_lfsmu_max	100	[%]	Max. additional power LFSM-U (dP > 0)
ddP_lfsmu_max	100	[%/s]	Max. rate of change in dP LFSM-U

Table A4. Power Source.

Name	Value	Unit	Description
Tgen_up	0.01	[s]	Generator max. ramp up time
Tgen_down	0.01	[s]	Generator max. ramp down time
Ctrl_side	0		Power control at: 0 = generator side, 1 = grid side
Kp	1		Proportional gain, power controller
Ti	10	[s]	Integrator time constant, power controller
mpp	0		Max. available power: 0 = p_max, 1 = inital power
p_min	0	[p.u.]	Minimum power
p_max	0.9	[p.u.]	Maximum rated powe

References

1. IRENA. *Renewable Capacity Statistics 2024*; International Renewable Energy Agency: Abu Dhabi, United Arab Emirates, 2024.
2. Doherty, R.; Mullane, A.; Nolan, G.; Burke, D.J.; Bryson, A.; O'Malley, M. An assessment of the impact of wind generation on system frequency control. *IEEE Trans. Power Syst.* **2009**, *25*, 452–460. [CrossRef]
3. Carrasco, J.M.; Franquelo, L.G.; Bialasiewicz, J.T.; Galvan, E.; PortilloGuisado, R.; Prats, M.A.M.; Leon, J.I.; Moreno-Alfonso, N. Power-electronic systems for the grid integration of renewable energy sources:a survey. *IEEE Trans. Ind. Electron.* **2006**, *53*, 1002–1016. [CrossRef]
4. Kundur, P.; Paserba, J.; Ajjarapu, V.; Andersson, G.; Bose, A.; Canizares, C.; Hatziargyriou, N.; Hill, D.; Stankovic, A.; Taylor, C.; et al. Definition and Classification of Power System Stability IEEE/CIGRE Joint Task Force on Stability Terms and Definitions. *IEEE Trans. Power Syst.* **2004**, *19*, 1387–1401.
5. Tina, G.M.; Maione, G.; Licciardello, S.; Stefanelli, D. Comparative Technical-Economical Analysis of Transient Stability ImproveImprovements in a Power System. *Appl. Sci.* **2021**, *11*, 11359. [CrossRef]
6. Tina, G.M.; Maione, G.; Licciardello, S. Evaluation of technical solutions to improve transient stability in power systems with wind power generation. *Energies* **2022**, *15*, 7055. [CrossRef]
7. Banshwar, A.; Sharma, N.K.; Sood, Y.R.; Shrivastava, R. Renewable energy sources as a new participant in ancillary service markets. *Energy Strategy Rev.* **2017**, *18*, 106–120. [CrossRef]
8. Survey on Ancillary Services Procurement Balancing Market Design 2021; ENTSO-E, WGAS 20 June 2022. Available online: https://eepublicdownloads.blob.core.windows.net/public-cdn-container/clean-documents/mc-documents/balancing_ancillary/2022/2022-06-20_WGAS_Survey.pdf (accessed on 5 October 2024).
9. Lin, Y.; Eto, J.H.; Johnson, B.B.; Flicker, J.D.; Lasseter, R.H.; Pico, H.N.V.; Seo, G.-S.; Pierre, B.J.; Ellis, A.; Miller, J.; et al. Pathways to the next-generation power system with inverter-based resources: Challenges and recommendations. *IEEE Electrif. Mag.* **2022**, *10*, 10–21. [CrossRef]
10. Akram, U.; Nadarajah, M.; Shah, R.; Milano, F. A review on rapid responsive energy storage technologies for frequency regulation in modern power systems. *Renew. Sustain. Energy Rev.* **2020**, *120*, 109626. [CrossRef]
11. Zhai, Q.; Meng, K.; Dong, Z.Y.; Ma, J. Modeling and analysis of lithium battery operations in spot and frequency regulation service markets in Australia electricity market. *IEEE Trans. Ind. Inform.* **2017**, *13*, 2576–2586. [CrossRef]
12. Ørum, E.; Kuivaniemi, M.; Laasonen, M.; Bruseth, A.I.; Jansson, E.A.; Danell, A.; Elkington, K.; Modig, N. *Future System Inertia*; Technical Report; ENTSOE: Brussels, Belgium, 2015; pp. 1–58.
13. Spahic, E.; Varma, D.; Beck, G.; Kuhn, G.; Hild, V. Impact of reduced system inertia on stable power system operation and an overview of possible solutions. In Proceedings of the 2016 IEEE Power and Energy Society General Meeting (PESGM), Boston, MA, USA, 17–21 July 2016; pp. 1–5.
14. Unruh, P.; Nuschke, M.; Strauß, P.; Welck, F. Overview on grid-forming inverter control methods. *Energies* **2020**, *13*, 2589. [CrossRef]
15. Grid-Forming Technology in Energy Systems Integration, Report by the Energy Systems Integration Group's High Share of Inverter-Based Generation Task Force, March 2022. Available online: https://www.esig.energy/wp-content/uploads/2022/03/ESIG-GFM-report-2022.pdf (accessed on 20 October 2024).
16. Hu, Q.; Han, R.; Quan, X.; Wu, Z.; Tang, C.; Li, W.; Wang, W. Grid-Forming Inverter Enabled Virtual Power Plants With Inertia Support Capability. *IEEE Trans. Smart Grid* **2022**, *13*, 4134–4143. [CrossRef]
17. Lasseter, R.H.; Chen, Z.; Pattabiraman, D. Grid-Forming Inverters: A Critical Asset for the Power Grid. *IEEE J. Emerg. Sel. Top. Power Electron.* **2020**, *8*, 925–935. [CrossRef]
18. Berizzi, A.; Bosisio, A.; Ilea, V.; Marchesini, D.; Perini, R.; Vicario, A. Analysis of Synthetic Inertia Strategies from Wind Turbines for Large System Stability. *IEEE Trans. Ind. Appl.* **2022**, *58*, 3184–3192. [CrossRef]
19. Zarina, P.P.; Mishra, S.; Sekhar, P.C. Deriving inertial response from a non-inertial PV system for frequency regulation. In Proceedings of the 2012 IEEE International Conference on Power Electronics, Drives and Energy Systems (PEDES), Bengaluru, India, 16–19 December 2012; pp. 1–5.
20. Xin, H.; Liu, Y.; Wang, Z.; Gan, D.; Yang, T. A New Frequency Regulation Strategy for Photovoltaic Systems Without Energy Storage. *IEEE Trans. Sustain. Energy* **2013**, *4*, 985–993. [CrossRef]

21. Rehman, H.U.; Yan, X.; Abdelbaky, M.A.; Jan, M.U.; Iqbal, S. An advanced virtual synchronous generator control technique for frequency regulation of grid-connected PV system. *Int. J. Electr. Power Energy Syst.* **2021**, *125*, 106440. [CrossRef]
22. Alsharif, H.; Jalili, M.; Hasan, K.N. A Comparative Analysis of Centralised vs. Distributed Battery Energy Storage System in Providing Frequency Regulation. In Proceedings of the 2021 IEEE PES Innovative Smart Grid Technologies—Asia (ISGT Asia), Brisbane, Australia, 5–8 December 2021; pp. 1–5.
23. Maione, G.; Morey, P.; Carpita, M.; Bozorg, M.; Tina, G.M. Dynamic Analysis of Future Scenarios of Power Systems Dominated by Inverter-Based Renewable Resources. In Proceedings of the 2023 International Conference on Clean Electrical Power (ICCEP), Terrasini, Italy, 27–29 June 2023; pp. 540–545.
24. Mohammad, Y.; Ghani, A. Determine Weakest Bus for IEEE 14 Bus Systems. *Int. J. Comput. Appl.* **2018**, *182*, 7–10. [CrossRef]
25. Adetokun, B.B.; Muriithi, C.M.; Ojo, J.O.; Oghorada, O. Impact assessment of increasing renewable energy penetration on voltage instability tendencies of power system buses using a QV-based index. *Sci. Rep.* **2023**, *13*, 9782. [CrossRef] [PubMed]
26. Iyambo, P.K.; Tzoneva, R. Transient stability analysis of the IEEE 14-bus electric power system. In Proceedings of the AFRICON 2007, Windhoek, South Africa, 26–28 September 2007; pp. 1–9.
27. Otuo-Acheampong, D.; Rashed, G.I.; Mensah, A.A.; Haider, H. Three-phase fault analysis of power system transient stability based on TCSC controller using FPA for its location. *J. Phys. Conf. Ser.* **2023**, *2467*, 012014. [CrossRef]
28. Kabra, P.N.; Donepudi, S.R. Power quality improvement and analysis of interconnected bus system with PMU using VSM-STATCOM. *Int. J. Appl.* **2022**, *11*, 52–61. [CrossRef]
29. DigSilent. *PowerFactory, Example from Literature, Documentation "Description of the 14 Bus System"*; DigSilent: Gomaringen, Germany, 2018.
30. WECC Solar Plant Dynamic Modeling Guidelines, 2014. Available online: https://it.scribd.com/document/368012945/WECC-Solar-Plant-Dynamic-Modeling-Guidelines (accessed on 16 October 2024).
31. DER_A. DER_A Benchmark Test. Available online: https://www.wecc.org/sites/default/files/documents/meeting/2024/CMPLDWg+DER_A-Benchmark_Test_protocol.pdf (accessed on 16 September 2024).
32. PowerFactory TechRef—Grid-Forming—Converter. Available online: https://www.google.com/url?sa=t&source=web&rct=j&opi=89978449&url=https://www.scribd.com/document/502919510/PowerFactory-TechRef-Grid-forming-Converter&ved=2ahUKEwjC9Z6EyOyJAxW9UGcHHVTYGOgQFnoECBgQAQ&usg=AOvVaw3-mXof3RayCGoLACnhDyxb (accessed on 29 October 2024).
33. Terna, Allegato A. 68 Centrali Fotovoltaiche. Condizioni Generali di Connessione Alle Reti AT, Sistemi di Protezione Regolazione e Controllo. Marzo 2023. Available online: https://download.terna.it/terna/Allegato_A68_20230320_8db29f1d29ec6e8.pdf (accessed on 8 November 2024).
34. CEI 0-16, Regola Tecnica di Riferimento per la Connessione di Utenti Attivi e Passivi Alle Reti AT ed MT Delle Imprese Distributrici di Energia Elettrica 2022-03. Available online: https://www.certifico.com/impianti/337-documenti-impianti/documenti-impianti-riservati/5591-cei-0-16 (accessed on 3 November 2024).
35. Entso-e. *Inertia and Rate of Change of Frequency (RoCoF), Version 17*; ENTSO-e: Brussels, Belgium, 2020.
36. Terna, Allegato 12, Criteri di Taratura dei Relè di Frequenza del Sistema Elettrico e Piano di Alleggerimento, Marzo 2020. Available online: https://download.terna.it/terna/Allegato%20A.12_8d7c12206bf176c.pdf (accessed on 1 October 2024).
37. ENTSOe. *SYSTEM DEFENCE PLAN SPD—Inertia TF*; ENTSOe: Brussels, Belgium, 2022.